Determining the Spatial Scale of Wave Variance for the Siting of Wave Energy Converters in Near Shore Coastal Environments

By

Landung Setiawan

May 31, 2015

Advisor: Miles Logsdon, Ph. D.

Senior Thesis Manuscript

Bachelor of Science in Oceanography

June 12, 2015

University of Washington

College of the Environment

School of Oceanography

1503 NE Boat Street

Ocean Teaching Building (OTB)

Seattle, WA 98105

landungs@uw.edu

Acknowledgement

I would like to sincerely thank Miles Logsdon for the guidance and support throughout the whole research process. I would also like to thank Alexandra Russell, Danny Grünbaum, David Thoreson, and Jon Morgan for their help and dedication, and recognize my fellow classmates for their words of advice. Lastly, I would to thank Darian Disrud for keeping me level-headed, calm, and sane at times of frustration.

Abstract

Oceanic surface waves are one of the biggest potential energy sources available to support our ever-increasing energy demands. The construction, development, and siting of large Wave Energy Converters in isolated regions are often expensive. This paper assesses a low cost and low energy alternative for wave energy research. An investigation of the spatial scale of the variability in the normalized surface wave heights (NSWHs) was performed to understand the extent of the underlying processes that control wave behavior. The variability is measured by the variance in the NSWHs at each observed paired locations along a near-shore coastal environment. Determination of the spatial scale is achieved when NSWHs are seen to be dissimilar between observed pairs of simultaneous measurement at different spatial lags. This variation is due to the separate processes that control the environment at those unique locations. Two wave buoys at different distances apart or spatial lags were designed, built, and implemented to answer the question of spatial scale variance. The buoys were deployed in central Puget Sound on a south facing, low-lying coastal, near-shore beach. A comparison between a Geostatistical (Kriging) and Deterministic (Inverse Distance Weighted) solution for spatial interpolation suggests that the processes governing waves are non-stationary, and exhibits multiple spatial scales over the spatial extent of only a few hundred meters. Additional research and development of this investigation technique will further our understanding of the underlying processes, and assist in the determination of optimum siting for Wave Energy Converters at commercial viable scales.

Introduction

In order to support the ever-increasing energy demands of society, alternate sources of energy are investigated. Oceanic surface waves are considered as a potential energy source, which are available to be exploited (Falnes 2007; Kim et al. 2012). In 2013, the average annual electricity consumption of U.S. residential utility is about 10,908 kWh. The west coast of United States has an estimated recoverable wave energy of about 250 TWh per year, which is about $9x10^{14}$ kJ per year (Minerals Management Service 2006; Epri 2011). The amount of electrical energy from waves could power about 23 million households, assuming 100% of efficiency and no power loss. This potential of a sustainable energy future has motivated many scientists and engineers alike to develop efficient and effective wave energy converters (WECs), in order to utilize surface wave potential. The development of WECs proposes important questions regarding their siting in the marine environment. Notwithstanding issues of environmental impacts, issues of economic concern pertaining to the transmission of harnessed energy and cost of large scale infrastructure must be considered. The costs of construction, deployment, and maintenance of these high power output WECs are often exorbitant. Furthermore, testing and implementing WECs in isolated regions of the world with harsh conditions has halted additional developments of these WECs (Falcão 2010). Regions that are isolated from the population would cause an increase in the cost for transmission of power, storage, and minimize accessibility.

An alternative solution to the siting of these WECs is low-energy, highly populated regions near the coast. These regions will lower the cost of transmissions, allow for smaller and cheaper design of WECs, and increase their accessibility. Additionally, a smaller infrastructure will decrease the carbon footprint left from the manufactured materials to produce these WECs.

In order to continue with this approach, further research is implemented on different near-shore coastal regions.

This study investigates the spatial scale of the variability in the normalized surface wave heights (NSWHs) in hopes of understanding the extent of the underlying processes that control wave behavior. The variability is measured by the variance in the NSWHs at each observed paired locations. The spatial scale is achieved when NSWHs are dissimilar due to the separate processes that control the environment at that location (Sen 1989; Altunkaynak and Özger 2005).

Wave measurements were collected in central Puget Sound at a coastal, south-facing Northern latitude beach. Puget Sound is a fjord estuary located in North Western region of Washington State, and was carved by the Puget Lobe from the Cordilleran ice sheets (Porter and Swanson 1998). The study area consists of a beach front with fairly flat bathymetry with a depth of about 20m and a constant decreasing slope; which creates a simpler model of the ocean shallow water wave dynamics. This study investigates approximately 400 meters associated with the highly populated urban city of Edmonds, Washington, a city of forty thousand people. It is an ideal site due to the variation in the topography of the beachfront, the highly populated region, and its location in a near-shore low-lying coastal environment (Bassett et al. 2011).

Two wave buoys were deployed at different distances apart (spatial lags) to obtain *in situ* wave motion measurements utilizing nine degrees of freedom inertial motion unit (IMU) technologies. These wave buoys were designed, built, and implemented for the purpose of this research to allow for rapid deployment, repeated observations, and high temporal sampling and a variety of spatial scales. This paper reviews the instrument design and analysis method used to evaluate the fine spatial scale wave behavior and the potential for siting wave energy converters at those scales.

Methods

Design Parameters – Two buoys and their electronic sensors were engineered for this study. Both buoy systems needed to be cost effective (under $500 in total), easily deployable and retrievable, able to gather accurate motion data, and be waterproof. These four underlying principles become the scope of the wave buoys. There are two ways that oceanic waves can be measured, directionally or non-directionally. Each approach of measurement results in different buoy and sensor designs (Bender et al. 2010; Herbers et al. 2012). Non-directional measurement is an Eulerian measurement at which data are collected from a fixed location. This limits the data spatially, and in the case of waves, only vertical motion would be recorded, while horizontal motion is constrained. In contrast, directional measurement is Lagrangian and follows the wave vertically and horizontally. In this research, the non-directional approach is utilized to measure wave heights.

An alternative method is the use of a pressure sensor to detect the change of pressure when a wave passes a fixed location. The challenge and potential drawback with the pressure sensor design is the placement upright on the unknown sediment at the seabed and the difficult in rapid deployment for repeated observation. For these reasons, the sensors for the wave buoys utilized nine degrees of freedom inertial motion unit (IMU) technologies.

Prototype – For the initial prototype of the sensors for the wave buoys, Arduino microcontrollers with XBee and SD shields were used to provide wireless communication from the sensors to the computer. This would allow the computer host to acquire information about the sensor status and record a large amount of data streaming simultaneously using the third party software CoolTerm (ver. 1.4.5). The data were also stored simultaneously onto a 16GB Micro SD card to prevent data losses from missed data packets when sent wirelessly through the XBee

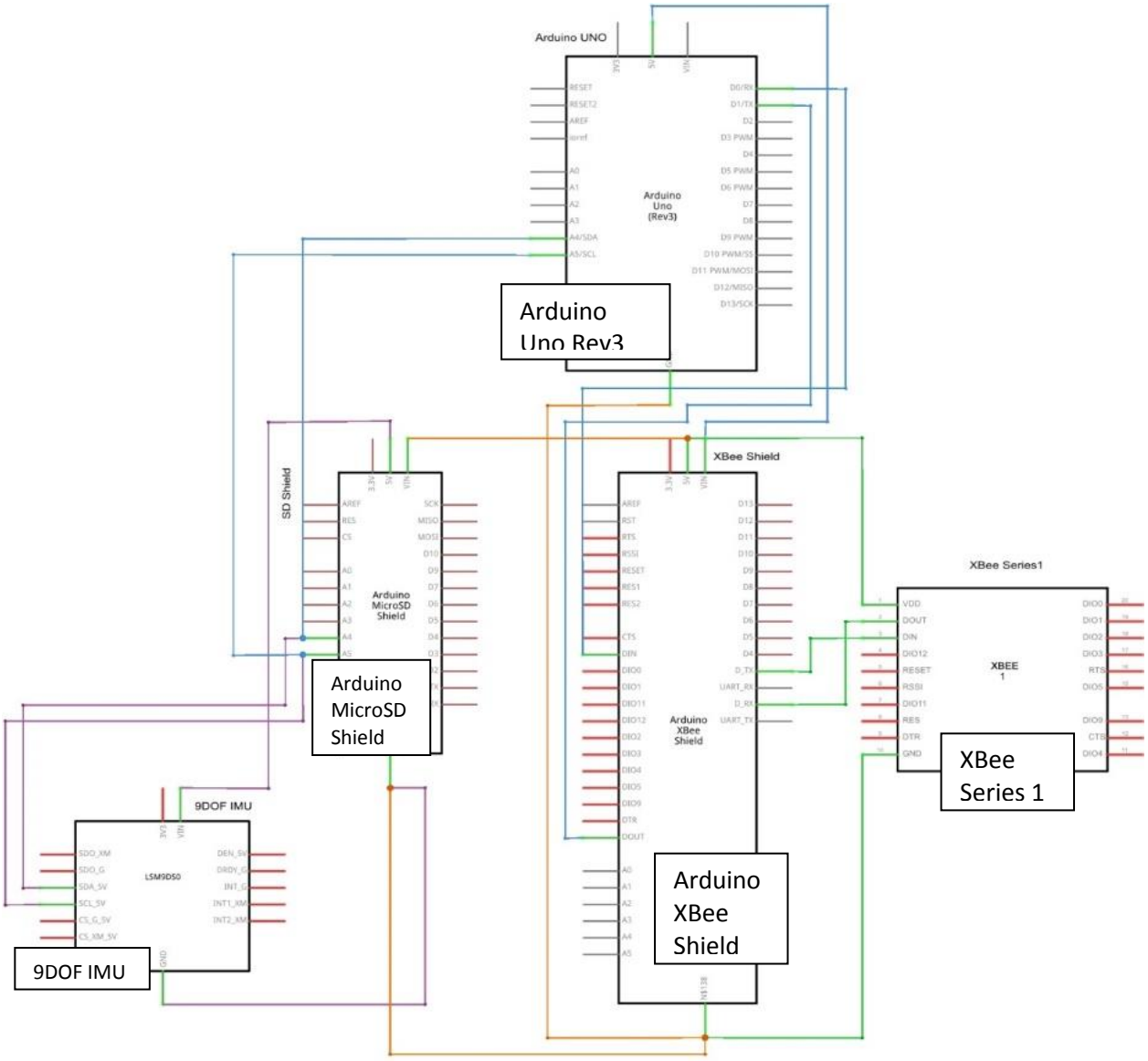

Figure 1. Schematic diagram of the wave sensor. Arduino Uno microcontroller is utilized to acquire acceleration and orientation from the 9-DOF IMU. Xbee wireless communication is used to transfer data from the two wave sensors live to a central computer to ensure that the wave sensors still works . Additionally, the data is logged into a 16GB MicroSD card using a microSD shield.

(Figure 1). The sensors were set to obtain the data with a 9600 baud rate. The nine degrees of freedom IMUs in each buoy was recording gyroscope rotations and accelerations in three axes. The change in position in the z-direction was calculated using calculus double integration method from the obtained gyroscope and acceleration data.

In order to keep the electronic sensor packages waterproof, they were placed inside the Pelican 1020 Micro case series, rated to be submerged under one meter of water for 30 minutes.

The sensor package was placed on top of a flange with surrounding floats. The complete wave buoy package was about 13” in diameter, measuring at the top. A 12” rod and two pound lead weight was attached to the bottom of the sensor package to stabilize the buoy and prevent it from inverting due to large wave surges (Figure 2). The sensor is 3” from the waterline to closely match the movement of the water surface. This entire wave buoy sensor package was tethered to a larger flotation buoy that is directly anchored to the seabed with 20 pounds of lead weight.

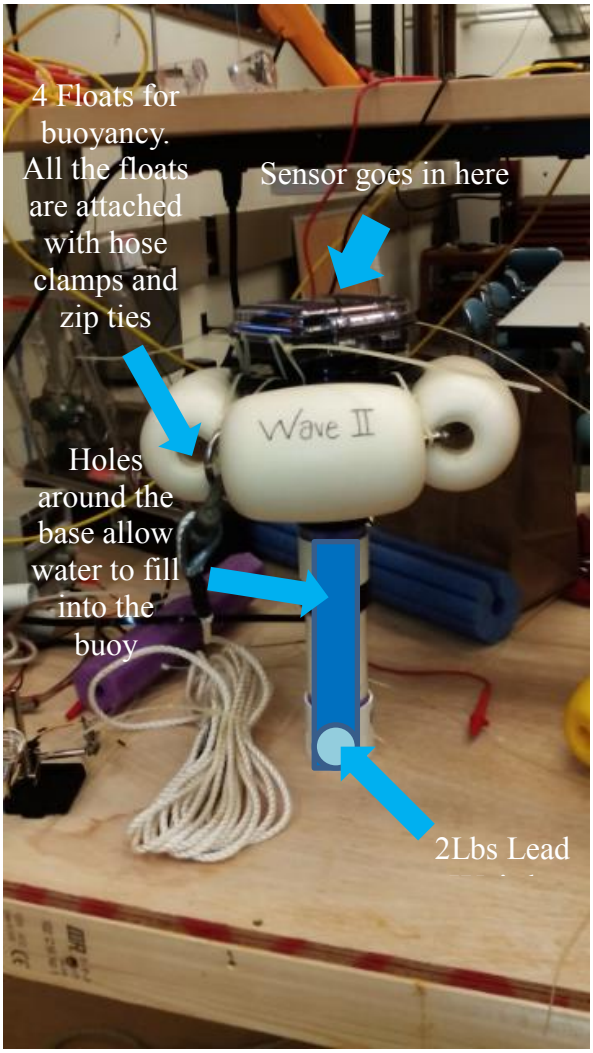

Figure 2. The final product of how everything was assembled is shown. The white rope on the left corner below the buoy will be used to attach the sensor buoy on to the large flotation buoy.

The prototype was deployed at Portage Bay off the dock of the University Of Washington School Of Oceanography on the R/V Barnes. The two buoys were floating about 17 meters apart and recorded motion data for approximately one hour (Figure 3). This distance apart represents one spatial lag while many spatial lags will be used in the final field deployment.

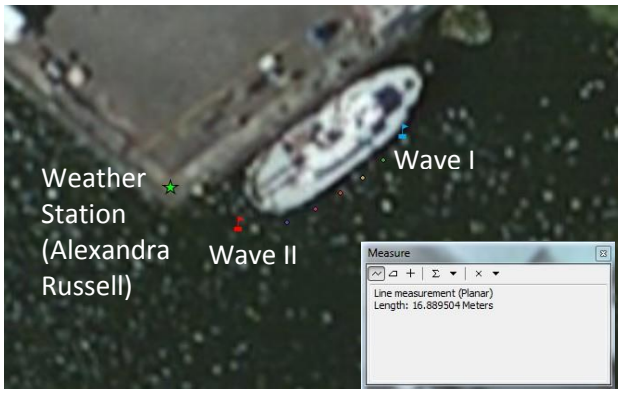

Figure 3. Seen are the two wave buoys at one distance apart for the field trial (Flag Markers). Their distance between them was approximately 16.89 meters. The colored dots represents lags from the “central buoy”, Wave II. This would be how the wave motion sensor will be placed during the actual field data collection.

Alternate Design – A watertight sphere buoy design was evaluated as an alternate design for this study. This design was to allow the buoy to follow the full motion of the water. In deep water (depth $h>\lambda/4$) water particles travel in circular orbits with them moving forward in crest and backward in the troughs. The radius of these movements decays exponentially with depth (Barber et al. 2009). This sphere design is best for capturing the full motion of the wave rather than only the z-component of the wave motion. Therefore, this alternate design was not applied in the research, but considered appropriate for other research area in full wave motion.

Final Design - Many design adjustments were needed as a result of the trial run using the prototype buoy. The XBee communication did not work while the sensors were on the water. So, for the final product of the wave buoy, the XBee shield was eliminated. This prevented communication with the wave sensors during the field expedition, but also increased battery life for all other electronics. The final design of the wave buoys had a sampling rate of 2 Hz and 115600 baud rate; it utilizes the Adafruit sensor, LSM303_Unified, and 9DOF libraries (Appendix A). Moreover, anchors were placed at the bottom of the line for each of the buoys along with the 20 Lbs. lead weight; this minimized the drift from currents and waves, allowing an accurate non-directional measurement. The recorded motion data for each buoy were stored onto the 16GB MicroSD card for further analysis. The whole electronic package was powered by a 9V battery in each buoy (Appendix B). Silicone packets were placed inside the pelican case along with the electronic package to keep the inside of the case to be dry.

Deployment - The final wave buoys were deployed on a south facing coastal beach in the Puget Sound region near the Port of Edmonds in Washington State. The deployment of the buoys was done as a small boat operation provided by the UW School of Oceanography. The first wave buoy (WAVE I) was powered on, time recorded then deployed into the water at station 1 (Figure 4). The same initialization method was performed with the second wave buoy (WAVE II) which was placed at station 2 and a 15 minute simultaneous data gathering period was begun. The steps of deployment and retrieval were repeated at each station along the 400m of beach front at spatial intervals away from WAVE I buoy as to create a set of paired temporal

Station	Lat	Long
1	47.807	-122.396
2	47.80667	-122.397
3	47.80625	-122.397
4	47.80581	-122.397
5	47.80547	-122.398
6	47.80503	-122.398
7	47.80436	-122.398
8	47.80378	-122.399

Table 1. This table shows the coordinates location of each Station, where wave motion buoys are deployed.

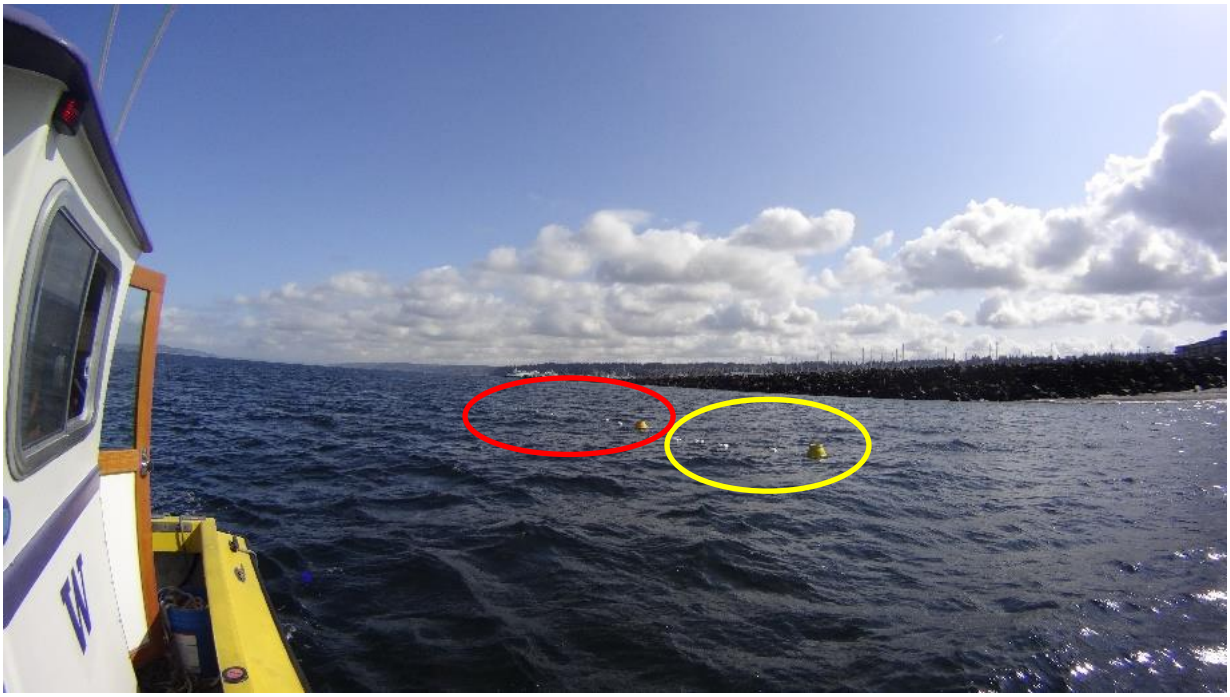

Figure 4. Shown in red circle is WAVE I and yellow circle is WAVE II. They are spaced apart during the first round of deployment.

observation at a verity of spatial lags (Table 1). After three hours of deployment, both wave buoys were retrieved and the recorded data in the SD card were uploaded into a computer for further processing.

Data Processing – The collected field data were organized and edited to remove periods of transition when the second buoy was in transit to its new location. Geographic coordinates from a handheld GPS at each deployment location was recorded and used as the spatial component of the data representation in the ESRI ArcGIS (ver. 10.1.) Geographic Information System (GIS) software. The synchronized motion data (raw gyroscope and accelerometer data) was then separated into the individual distance lags in a comma separated variable (CSV) file and uploaded to MATLAB for further analysis. Velocity terms were calculated by performing integration to the raw acceleration data. From there, an integration of the velocity data would result in position of the wave or the sea level height. Butterworth filter was also used to remove natural electronic drift in the sensor. The significant wave height (Hs) was calculated for each distance lags. Significant wave height is defined as the average of the highest 1/3 of the waves, as measured from the trough to the crest of the waves. Note that H_s is significant wave height in meters, W_v is variance of wave displacement.

$$H_s = 4 \cdot \sqrt{W_v} \quad [1]$$

From the calculated significant wave height, power can be calculated by using the wave power equation. Note that P is power in kW/m, H_s is significant wave height in meters, and T is wave period.

$$P = 0.57 \cdot H_s^2 T \quad [2]$$

A MATLAB script was used to perform the calculations and plotting for all of the data (Appendix C). The resulting significant wave height data was normalized by dividing the

significant wave height of WAVE II by the significant height of WAVE I at each of the paired distance lag. The compiled data were then combined with the GPS for coordinates and plotted as spatial data objects with attributes of the normalized significant wave height (NSWH) in the GIS.

Spatial Analysis – A technique often used in spatial analysis to model regionalized variables is the cumulative semivariogram; which is the summation of one half the squared differences in paired observations, and then ranked according to ascending order of distances between samples within a region (Sen 1989). This allows a visual creation of a variance versus distance plot. The hypothesis states that wave height semivariance between the two sensors will increase as the distance between their paired observations increases until the distance apart in the observations begin to explain less of the variance in the observed measurements. At that distance (the spatial range) where variation is no longer correlated with increased distance apart, the underlying spatial "scale" has been exceeded. From this perspective, the spatial scale of normalized significant wave height (NSWH) variance is equal to the maximum measured distance separating the two sensors, which exhibit the maximum variance as a function of separation (Figure 5). At the spatial scale, the differences between the two locations are very distinct, which concluded that each buoy is at its own distinct environment, where individual processes are occurring.

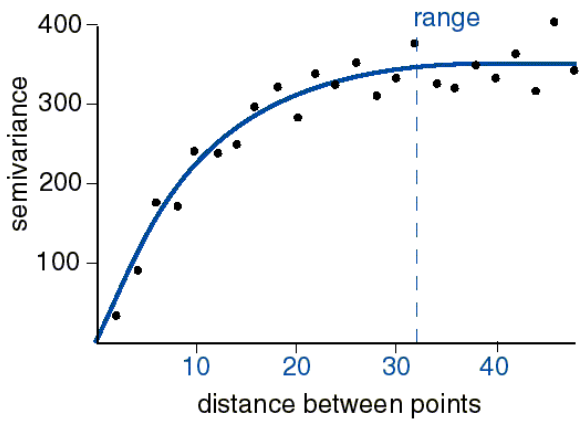

Figure 5. An example of a semivariogram which shows the range, the spatial "scale". The axes are semivariance versus distance between points.

In ArcGIS, the NSWH for each station was converted into point vector shape file and plotted on the map. The original

coordinate system of these points was World WGS 1984. The coordinates was then converted into projected coordinate system of UTM WGS 1984 Zone 10N. This conversion changes the horizontal measurement unit from the geographic decimal degrees into projected Mercator meters. From the NSWH data, two different interpolation methods were used to determine the overall wave heights over the extent of the study area. These interpolation methods were Ordinary Kriging and Inverse Distance Weighted (IDW). Additionally, analysis of the empirical semivariogram was performed to determine the spatial scale of the NSWH variance using the Geostatistical wizard in ArcGIS.

Kriging – Kriging is a Geostatistical method of interpolation to estimate values in an unknown location within the spatial scale (Isaaks 1989; Cressie 1993). This method is based on the cumulative semivariance. When the Kriging solution is used to determine a fitted model to the semivariance an interpolated map of the predicted values based on the few measured values may be produced. This aids in the visualization of the spatial variability of the NSWH along the coastline. Performing ordinary Kriging with a Spherical semivariogram model created an interpolated surface of the NSWH. The average lag size of each of the distance lags was calculated in Excel. This average lag size was used to set the lag size for the Kriging model and the neighboring point requirement was set to eight to insure all stations were represented. The interpolated surface was represented as a continuous raster surfaces with an output cell size of 5m.

IDW – Inverse distance weighted is a deterministic method of interpolation, in contrast with the stochastic Kriging method. This interpolation method determines the NSWH values in a cell linearly. This linear weight function is the inverse of distance and may be set as a square of distance by assigning a power setting to the distance decay function such that the influence of

one sample on another decreases with the square of distance. Again, a minimum number of neighboring points may be defined to ensure representation of all neighbors. A 5m grid cell raster of the IDW interpolated surface was constructed using the default power of 2 for the distance decay function, and the number of neighboring points set to eight.

SignificantWave HeightI(m)	WavePeriod I(s)	PowerI (kW/m)	SignificantWave HeightII(m)	WavePeriod II(s)	PowerII (kW/m)	Distance Lag(m)	Lag
2.284742679	1.039898256	3.094142378	2.183499978	1.043138686	2.834805663	44.668242	1
2.38946414	1.018849057	3.315780229	2.15958999	1.062225519	2.823801719	59.579231	2
2.309913119	1.072891278	3.26303597	2.28244812	1.038199768	3.082887046	49.738109	3
2.355004567	1.046713287	3.308918726	2.221634884	1.035806452	2.914062348	49.833029	4
2.408552049	1.066868186	3.527749122	2.237731633	1.035009615	2.95416836	49.389703	5
2.279225652	1.059375736	3.136891705	2.27271139	1.074598802	3.163805559	74.133599	6
2.461896495	1.056943005	3.651455436	2.180366728	1.031053698	2.793928143	99.023374	7

Table 2. This table shows the results from the calculations and data arrays of each paired observation distance lags. Note that the red text is the observed highest significant wave height and the blue text is the lowest.

Results

Buoy Design – The buoy and sensor design aspect of this research was a success. The wave buoys did not drift from their locations and the electronics were dry and performed flawlessly for the whole duration of the deployment. The floats were able to follow the vertical movement of waves, and were not dampened in their vertical motion. The resulting calculated data showed variability in the wave heights between the two buoys (Appendix D.I). Additionally, natural electronic sensor drift seen in the linear velocity was completely removed via the Butterworth filter (Appendix D.II).

Data analysis – The resulting significant wave heights (H_s) and periods (T) were different for each of the station. The highest H_s was observed at the location of WAVE I (Station 1, 47.807,-122.396), which was 2.46 meters between 13:26 to 13:43. The period of the observed wave was about 1.06 seconds. The power output, assuming 100% efficiency, at this location during that time interval would have been 3.65 kW/m. In contrast, the smallest H_s was observed at the location of WAVE II (Station 3, 47.806, -122.397), which was 2.16 meters between 11:46

to 12:04. The wave period was 1.06 seconds with the power output of 2.82 kW/m. Overall, Station 1 has higher significant wave heights compared to the other stations (Table 2). Within the whole study area, the average significant wave height was about 2.29 meters in a span of 3 hours and 14 minutes. The wave period was 1.05 seconds and the power output was 3.13 kW/m in this near-shore coastal environment.

Spatial analysis – The two different method of interpolation resulted in different raster surfaces. The Kriging method of interpolation (Geostatistical), resulted on a raster surfaced that are smoothed throughout the study area with only few hotspots, while the IDW (deterministic)

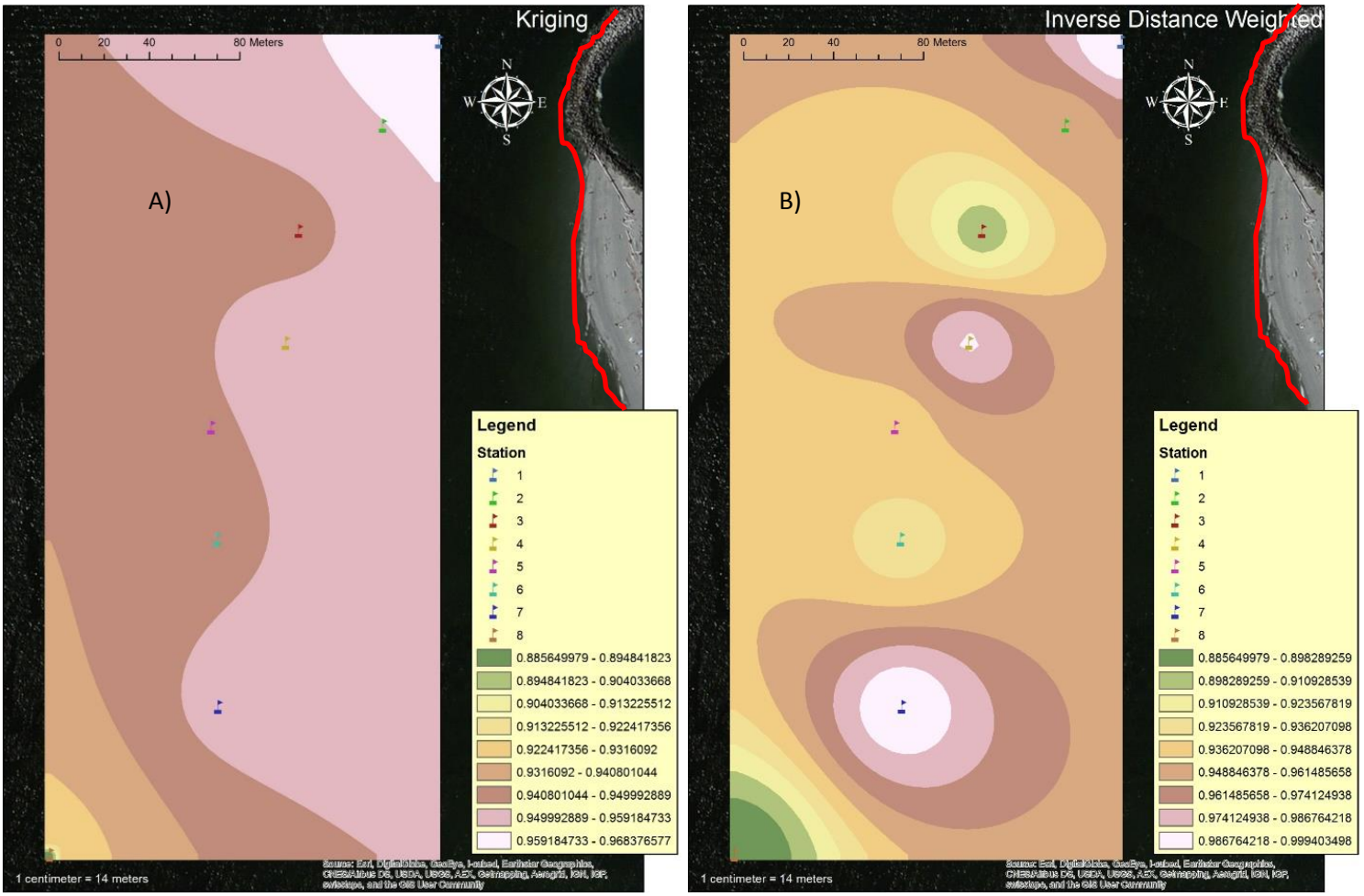

Figure 6. A) Kriging model surface within the study area. The Kriging surface reveals some areas that have similar processes, such as 3,5,6 and 4,7. Those areas have similar NSWH variability. B) IDW model surface within the study area. The IDW model reveals hotspots where areas are extremely different from the rest of the stations. Note that shoreline is highlighted in red. City of Edmonds is east of the shoreline.

portrays concentrated areas of wave motion at each buoy location. The Kriging interpolation produces a smoothed surface with some anomalies in the middle of the study area (Figure 6A). The IDW interpolation resulted in hotspot areas of either high NSWH or low NSWH, and the central of the study area alternates between areas of high and then low (Figure 6B).

The empirical semivariogram illustrates rapid change in increasing semivariance at a number of different spatial lags (Figure 7). The resulting data from the empirical semivariogram shows a high amount of variability at different distance lags. There are three distances at which the paired observations exhibit low variability. Average lag size was calculated from the lags between the 8 stations.

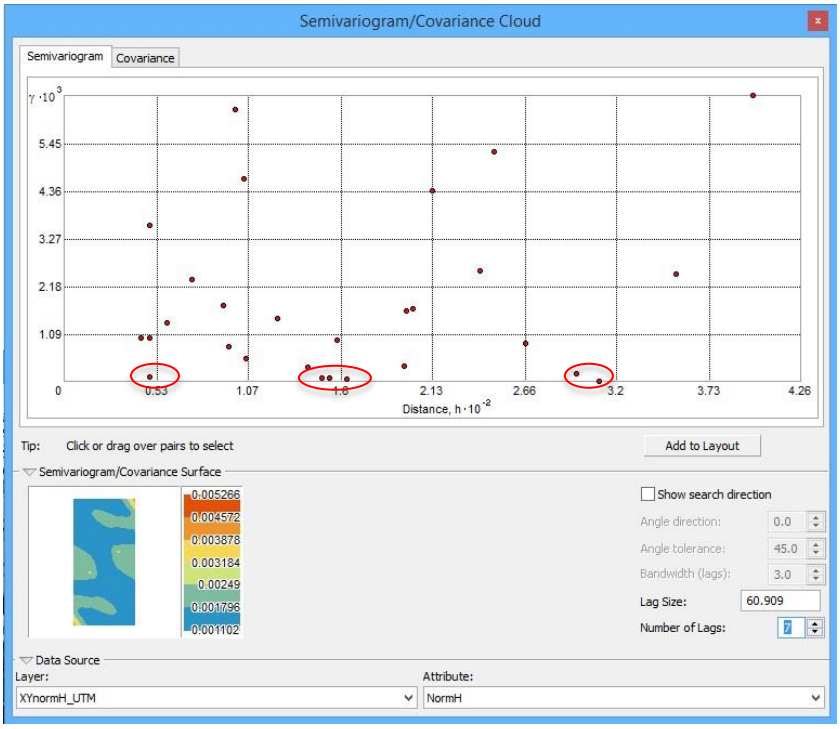

Figure 7. Empirical Semivariogram of the result from the study shows three distance lags with low variability circled in red. Lag size of 60.909 is the average distance lags within the study area.

Discussion

Though everything worked as designed, further calibration studies are needed for the IMU to be confirmed as an accurate data recording device. This IMU was not designed to record wave movements only in the z-direction, but mostly horizontal axes which might cause some source of errors. Additionally, the size of the buoy limited the type of waves that can be captured, which are waves with shorter wavelengths of about 13”. The placement of the electronic package on the

buoy (3” from waterline) could possibly affect the behavior of the buoy and alter the true measurement.

The observed significant wave height was highest at station 1 during the whole duration of the deployment. At this location the mean depth of the water was about 15m. This station was about 69 meters to shore, and since the wavelength of the recorded waves were about 13”, these waves do not feel the bathymetry and therefore some other factor such as wind must have caused this location to have the highest significant wave height . The smallest significant wave height observed was located about 128 meters from shore and was at a mean depth of about 13 meters. This location might have less wind, which in turn decrease the significant wave height by about 0.20 meters. Station 3 is about 104 meters from Station 1, and they are different from each other. This difference might be due to the spatial scale. There are a different process governing the two locations, this can be seen clearly in both the Kriging and IDW interpolated surface. Furthermore, this difference in significant wave heights can also be resulted from sensor calibration errors since the readings of wave buoy I z-acceleration were higher than wave buoy II (buoy I: ~10.00 m/s^2, buoy II: ~11 m/s^2).

Although the distance from Station 1 to Station 8 is only 398 meters, there are many processes that govern this area. These processes can be seen in all of the interpolated surfaces using either Geostatistical or deterministic interpolated solutions. The empirical semivariogram shows the distance lags at which these processes occur. Within the spatial extent of the study area, there are regions that have very different significant wave height as a function of distance apart. Therefore, at the three highlighted distance lags (50m, 140m, and 300m) there are different sets of processes that govern the wave height at those distances apart.

These measured observations when combined across all spatial lags assume that large scale difference due to time can be treated as uniform. In this way observations taken throughout the day are representative of paired observation of the same large scale processes controlling wave behavior. From this perspective, over the spatial extent of these samples the underlying process exhibits non-stationary in the process governing the significant wave height. However, assuming that the process is stationary, the spatial scale or range predicted by the Kriging surface is 487.272m. Therefore, the measured wave heights are within the larger spatial scale and it has not been exceeded. The waves are experiencing similar processes within this spatial extent.

Summary

Current research on wave energy often require scientists and engineers to travel to isolated places, under harsh conditions in order to implement Wave Energy Converters (WECs). Power transmission lines for these hard to reach WECs are often expensive. This study was conducted to investigate the low cost and low energy alternative for wave energy research. This in turn will lessen carbon footprint, be sustainable, and commercially viable. A determination of the spatial scale of the variability in wave height was performed, utilizing wave buoys set at different distances apart (spatial lags). The study area consists of a near-shore coastal environment, close to the populated city of Edmonds. The wave buoys used was designed, built, and implemented to capture wave motion by using 9 degrees of freedom technology. Raw gyroscope and acceleration data were collected and processed to give measurements of wave heights. Further calculation resulted in normalized significant wave heights for each of the buoys.

Spatial analysis was performed using two methods of interpolation, Kriging and Inverse Distance Weighted. Both surfaces show more than one process that governs the behavior of

waves within the study area. Therefore the underlying process is non-stationary, which can be observed in an empirical semivariogram of the data. Further study is needed to investigate these different processes. Since wave heights are also affected by winds and tides, a time-space semivariogram is needed in looking at how the spatial scale changes over time. Smaller spatial lags wave motion measurements are needed to investigate the scale of the stationary processes that occur within this study area. This will provide a more accurate model for the siting of WECs.

Further research into low-energy, near shore, coastal environment would be beneficial for the siting of wave energy converters. This research can be the stepping stone towards that development. A better wave buoy instrument is needed for the continuation of this research area. Once the underlying processes can be determined for these waves, the better it will be to predict areas that would be cost-effective, easy to access, and environmentally friendly.

References

Altunkaynak, A., and M. Özger. 2005. Spatial Significant Wave Height Variation Assessment and Its Estimation. J. Waterw. Port, Coastal, Ocean Eng. **131**: 277–282.

Barber, B. Y. N. F., F. Ursell, G. E. R. Deacon, and F. R. S. May. 2009. The Generation and Propagation Ocean Waves and Swell I . Wave Periods and Velocities. **240**: 527–560.

Bassett, C., J. Thomson, B. Polagye, and K. Rhinefrank. 2011. Underwater noise measurements of a 1 / 7 th scale wave energy converter.

Bender, L. C., N. L. Guinasso, J. N. Walpert, and S. D. Howden. 2010. A Comparison of Methods for Determining Significant Wave Heights—Applied to a 3-m Discus Buoy during Hurricane Katrina. J. Atmos. Ocean. Technol. **27**: 1012–1028.

Epri. 2011. Mapping and Assessment of the United States Ocean Wave Energy Resource. Power , doi:1024637

Falcão, A. F. D. O. 2010. Wave energy utilization: A review of the technologies. Renew. Sustain. Energy Rev. **14**: 899–918.

Falnes, J. 2007. A review of wave-energy extraction. Mar. Struct. **20**: 185–201.

Herbers, T. H. C., P. F. Jessen, T. T. Janssen, D. B. Colbert, and J. H. MacMahan. 2012. Observing Ocean Surface Waves with GPS-Tracked Buoys. J. Atmos. Ocean. Technol. **29**: 944–959.

Kim, C.-K., J. E. Toft, M. Papenfus, G. Verutes, A. D. Guerry, M. H. Ruckelshaus, K. K. Arkema, G. Guannel, S. a Wood, J. R. Bernhardt, H. Tallis, M. L. Plummer, B. S. Halpern, M. L. Pinsky, M. W. Beck, F. Chan, K. M. a Chan, P. S. Levin, and S. Polasky. 2012. Catching the right wave: evaluating wave energy resources and potential compatibility with existing marine and coastal uses. PLoS One **7**: e47598.

Minerals Management Service. 2006. Technology White Paper on Wave Energy Potential on the U.S. Outer Continental Shelf.

Porter, S. C., and T. W. Swanson. 1998. Radiocarbon Age Constraints on Rates of Advance and Retreat of the Puget Lobe of the Cordilleran Ice Sheet during the Last Glaciation. Quat. Res. **50**: 205–213.

Sen, Z. 1989. Cumulative semivariogram models of regionalized variables. Math. Geol. **21**: 891–903.

Appendix A. Sensor Code for the Arduino

```
/*                    INITILIZATION                          */
#include <Wire.h>

// 9 DOF
#include <Adafruit_Sensor.h>
#include <Adafruit_LSM303_U.h>
#include <Adafruit_9DOF.h>

#include <OneWire.h>
#include <SD.h>

// Assign a unique ID to the sensors
Adafruit_9DOF                dof   = Adafruit_9DOF();
Adafruit_LSM303_Accel_Unified  accel = Adafruit_LSM303_Accel_Unified(1111);
Adafruit_LSM303_Mag_Unified    mag   = Adafruit_LSM303_Mag_Unified(1112);

/* Update this with the correct SLP for accurate altitude measurements */
float seaLevelPressure = SENSORS_PRESSURE_SEALEVELHPA;

unsigned long start, finished, elapsed, count;

const int chipSelect = 8;

/*                    DATA AQUISITION                        */
void setup(void) {
        Serial.begin(115200);
        start=millis();
        count = 0;
        Serial.print("Wave I Initialize ");
        /* Initialise the sensors */
        initSensors();
        Serial.println("Initializing SD card...");
        // make sure that the default chip select pin is set to output, even if you don't use it:
        pinMode(chipSelect, OUTPUT);
        // see if the card is present and can be initialized:
        if (!SD.begin(chipSelect)) {
                Serial.println("Card failed, or not present");
                // don't do anything more:
                return;
        }
        Serial.println("card initialized.");

}
void initSensors() {
        if(!accel.begin()) {
                /* There was a problem detecting the LSM303 ... check your connections */
                Serial.println("Ooops, no LSM303 detected ... Check your wiring!");
                while(1);
        }
        if(!mag.begin()) {
                /* There was a problem detecting the LSM303 ... check your connections */
                Serial.println("Ooops, no LSM303 detected ... Check your wiring!");
                while(1);
        }
}
void loop(void) {
        File dataFile = SD.open("datalog.txt", FILE_WRITE);
        // 9 DOF
        sensors_event_t accel_event;
        sensors_event_t mag_event;
```

```
	sensors_vec_t   orientation;
	sensors_event_t event;
	accel.getEvent(&event);
	if (dataFile) {
		finished=millis();
		elapsed=finished-start;

		Serial.print("I,");
		dataFile.print("I,");

		Serial.print(elapsed/1000.0);
		dataFile.print(elapsed/1000.0);

		Serial.print(",");
		dataFile.print(",");

		Serial.print(count++);
		dataFile.print(count++);

		Serial.print(",");
		dataFile.print(",");

		/* Calculate pitch and roll from the raw accelerometer data */
		accel.getEvent(&accel_event);
		if (dof.accelGetOrientation(&accel_event, &orientation)) {
			Serial.print(orientation.roll);
			dataFile.print(orientation.roll); //Roll
			Serial.print(",");
			dataFile.print(",");
			Serial.print(orientation.pitch);
			dataFile.print(orientation.pitch); //Pitch
			Serial.print(",");
			dataFile.print(",");
		}
		/* Calculate the heading or "yaw" using the magnetometer */
		mag.getEvent(&mag_event);
		if (dof.magGetOrientation(SENSOR_AXIS_Z, &mag_event, &orientation)) {
			Serial.print(orientation.heading);
			dataFile.print(orientation.heading); //Yaw
			Serial.print(",");
			dataFile.print(",");
		}
		/* Display the results (acceleration is measured in m/s^2) */
		Serial.print(event.acceleration.x);
		dataFile.print(event.acceleration.x); // X Acceleration
		Serial.print(",");
		dataFile.print(",");
		Serial.print(event.acceleration.y);
		dataFile.print(event.acceleration.y); // Y Acceleration
		Serial.print(",");
		dataFile.print(",");
		Serial.print(event.acceleration.z);
		dataFile.print(event.acceleration.z); // Z Acceleration

		Serial.println("");
		dataFile.println("");
		dataFile.close();
	}
}
```

Appendix B. Schematic Diagram for the Final Sensor Design

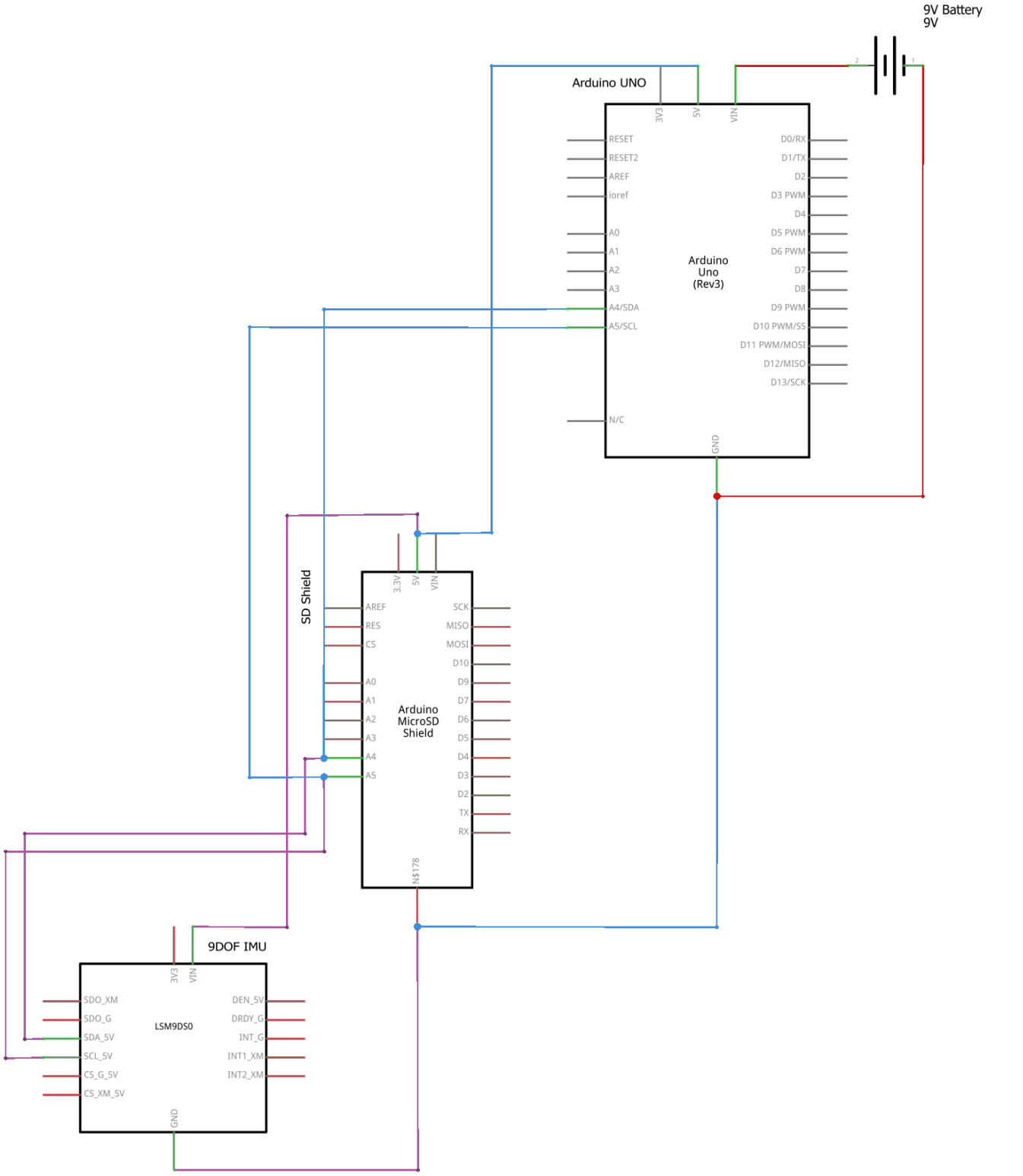

Appendix C. MATLAB Scripts for calculations and graphing

I. waveCalc.m

```
%This is the code for the raw calculations Function
function [position,tMod,avgperiod,sigwaveheight,power] = waveCalc(wave,fileName,...
ax,ay,az,gx,gy,gz,t)
%% Import data

rawdata = importdata(fileName);
IMUdata = rawdata;

samplePeriod = 1/2;

acc = [IMUdata(:,ax),IMUdata(:,ay),IMUdata(:,az)];          % accelerometer
gyr = [IMUdata(:,gx),IMUdata(:,gy),IMUdata(:,gz)];
time = IMUdata(:,t);

% time is changed to start from 0
tMod = zeros(length(time),1);
for kk = 1:length(time)-1
   tMod = time - time(1,1);
end
%% Calculations

% calculate orientation
R = zeros(3,3,length(gyr));     % rotation matrix describing sensor relative to Earth

for i = 1:length(gyr)
   R(1,1,i) = cos(gyr(i,3)).*cos(gyr(i,2));
   R(1,2,i) = (cos(gyr(i,3)).*sin(gyr(i,2)).*sin(gyr(i,1)))-(sin(gyr(i,3)).*cos(gyr(i,1)));
   R(1,3,i) = (cos(gyr(i,3)).*sin(gyr(i,2)).*cos(gyr(i,1)))+(sin(gyr(i,3)).*sin(gyr(i,1)));
   R(2,1,i) = sin(gyr(i,3)).*cos(gyr(i,2));
   R(2,2,i) = (sin(gyr(i,3)).*sin(gyr(i,2)).*sin(gyr(i,1)))+(cos(gyr(i,3)).*cos(gyr(i,1)));
   R(2,3,i) = (sin(gyr(i,3)).*sin(gyr(i,2)).*cos(gyr(i,1)))-(cos(gyr(i,3)).*sin(gyr(i,1)));
   R(3,1,i) = -sin(gyr(i,2));
   R(3,2,i) = cos(gyr(i,2)).*sin(gyr(i,1));
   R(3,3,i) = cos(gyr(i,2)).*cos(gyr(i,1));
end

% Calculate 'tilt-compensated' accelerometer

tcAcc = zeros(size(acc));  % accelerometer in Earth frame

for i = 1:length(acc)
   tcAcc(i,:) = R(:,:,i) * acc(i,:)';
end

% Calculate linear acceleration in Earth frame (subtracting gravity)

linAcc = tcAcc - [zeros(length(tcAcc), 1), zeros(length(tcAcc), 1), ones(length(tcAcc), 1)];

% Calculate linear velocity (integrate acceleration)

linVel = zeros(size(linAcc));

for i = 2:length(linAcc)
   linVel(i,:) = linVel(i-1,:) + linAcc(i,:) * samplePeriod;
end

% High-pass filter linear velocity to remove drift

order = 1;
filtCutOff = 0.1;
```

```
[b, a] = butter(order, (2*filtCutOff)/(1/samplePeriod), 'high');
linVelHP = filtfilt(b, a, linVel);

% Calculate linear position (integrate velocity)
linPos = zeros(size(linVelHP));

for i = 2:length(linVelHP)
    linPos(i,:) = linPos(i-1,:) + linVelHP(i,:) * samplePeriod;
end

% High-pass filter linear position to remove drift

order = 1;
filtCutOff = 0.1;
[b, a] = butter(order, (2*filtCutOff)/(1/samplePeriod), 'high');
linPosHP = filtfilt(b, a, linPos);
position = (linPosHP .* 0.40);

% Calculate Height and Avg. Height
height = zeros(length(position(:,3)),1);
for zz = 1:length(position(:,3)) - 1
    if linPosHP(zz,3) > 0
        height(zz,:) = linPosHP(zz,3);
    end
end

averageHeight = sum(height)/length(height);

%wave period calculation
buoyOne = [tMod,height];
remZero = buoyOne(:,2)==0;
buoyOne(remZero,:) = [];

% calculating change in time at every time step
period = zeros(length(buoyOne(:,1)),1);
for jj = 1:length(buoyOne(:,1))-1
    period(jj,1) = buoyOne(jj+1,1) - buoyOne(jj,1);
end

% calculate average period
avgperiod = mean(period);

% significant wave height
sigwaveheight = 4 * sqrt(var(position(:,3)));

% power kW/m
power = 0.57 * (sigwaveheight^2) * avgperiod;

%% Senior Thesis Graph
figure('Name', strcat(fileName,wave));

%raw accelerometer
subplot(3,4,[1 2]);
hold on;
plot(tMod,acc(:,1), 'r');
plot(tMod,acc(:,2), 'g');
plot(tMod,acc(:,3), 'b');
axis([0 900 -20 20]);
ylabel('m/s^2');
title('Accelerometer');
legend1 = legend('X', 'Y', 'Z');
set(legend1,'Position',[0.929233772571985 0.467726396917148 0.0490483162518301 0.0876685934489403]);
```

```
%tilt compesated accelerometer
subplot(3,4,3);
hold on;
plot(tMod,tcAcc(:,1), 'r');
plot(tMod,tcAcc(:,2), 'g');
plot(tMod,tcAcc(:,3), 'b');
axis([0 900 -20 20]);
ylabel('m/s^2');
title('"Tilt-compensated" accelerometer');

%linear acceleration
subplot(3,4,4);
hold on;
plot(tMod,linAcc(:,1), 'r');
plot(tMod,linAcc(:,2), 'g');
plot(tMod,linAcc(:,3), 'b');
axis([0 900 -20 20]);
ylabel('m/s^2');
title('Linear acceleration');

%linear velocity
subplot(3,4,7);
hold on;
plot(tMod,linVel(:,1), 'r');
plot(tMod,linVel(:,2), 'g');
plot(tMod,linVel(:,3), 'b');
axis([0 900 -800 800]);
xlabel('seconds');
ylabel('m/s');
title('Linear velocity');

%High-pass linear velocity
subplot(3,4,8);
hold on;
plot(tMod,linVelHP(:,1), 'r');
plot(tMod,linVelHP(:,2), 'g');
plot(tMod,linVelHP(:,3), 'b');
axis([0 900 -10 10]);
xlabel('seconds');
ylabel('m/s');
title('High-pass filtered linear velocity');

%linear position
subplot(3,4,[5 6]);
hold on;
plot(tMod,linPos(:,1), 'r');
plot(tMod,linPos(:,2), 'g');
plot(tMod,linPos(:,3), 'b');
axis([0 900 -30 30]);
xlabel('seconds');
ylabel('m');
title('Linear position');

%high-filtered position
subplot(3,4,[9 10 11 12]);
hold on;
plot(tMod,position(:,3), 'b');
axis([0 900 -2 2]);
xlabel('seconds');
ylabel('m');
title('High-pass filtered linear position');
```

```
hold off;
end
```

II. waveProcess.m

```
%The function that takes in the raw data, calling waveCalc function and gives out data array Results
function [Results] = waveProcess(file)

[position1, tMod1, avgPeriod1, sigwaveheight1, power1] = ...
waveCalc('_wave_1',file,6,7,8,3,4,5,1);
[position2, tMod2, avgPeriod2, sigwaveheight2, power2] = ...
waveCalc('_wave_2',file,14,15,16,11,12,13,9);

figure('Name', strcat(file,'_Position Data'));
hold on;
plot(tMod1,position1(:,1), 'r');
plot(tMod2,position2(:,2), 'g');
axis([0 900 -2 2]);
xlabel('time(seconds)');
ylabel('height(meters)');
title('High-pass filtered linear position');
legend1 = legend('Wave Buoy I', 'Wave Buoy II');
set(legend1,'Position',[0.143728648121013 ...
   0.142100192678225 0.0980966325036558 0.0606936416184971]);

Results = dataset({sigwaveheight1,'Significant Wave HeightI'},...
        {avgPeriod1,'Wave PeriodI'},...
        {power1,'PowerI'},...
        {sigwaveheight2,'Significant Wave HeightII'},...
        {avgPeriod2,'Wave PeriodII'},...
        {power2,'PowerII'});
End
```

III. Results.m

```
%This script exports the resulting data arrays to excel files
clear all; close all; clc

[resultLag1] = waveProcess('lag_1.csv');
export(resultLag1,'XLSFile','lag_1Results.xlsx')

[resultLag2] = waveProcess('lag_2.csv');
export(resultLag2,'XLSFile','lag_2Results.xlsx')

[resultLag3] = waveProcess('lag_3.csv');
export(resultLag3,'XLSFile','lag_3Results.xlsx')

[resultLag4] = waveProcess('lag_4.csv');
export(resultLag4,'XLSFile','lag_4Results.xlsx')

[resultLag5] = waveProcess('lag_5.csv');
export(resultLag5,'XLSFile','lag_5Results.xlsx')

[resultLag6] = waveProcess('lag_6.csv');
export(resultLag6,'XLSFile','lag_6Results.xlsx')

[resultLag7] = waveProcess('lag_7.csv');
export(resultLag7,'XLSFile','lag_7Results.xlsx')
```

Appendix D. Graph Results from Calculations in MATLAB.

I. Wave/Sea Level Heights Example from lag 4.

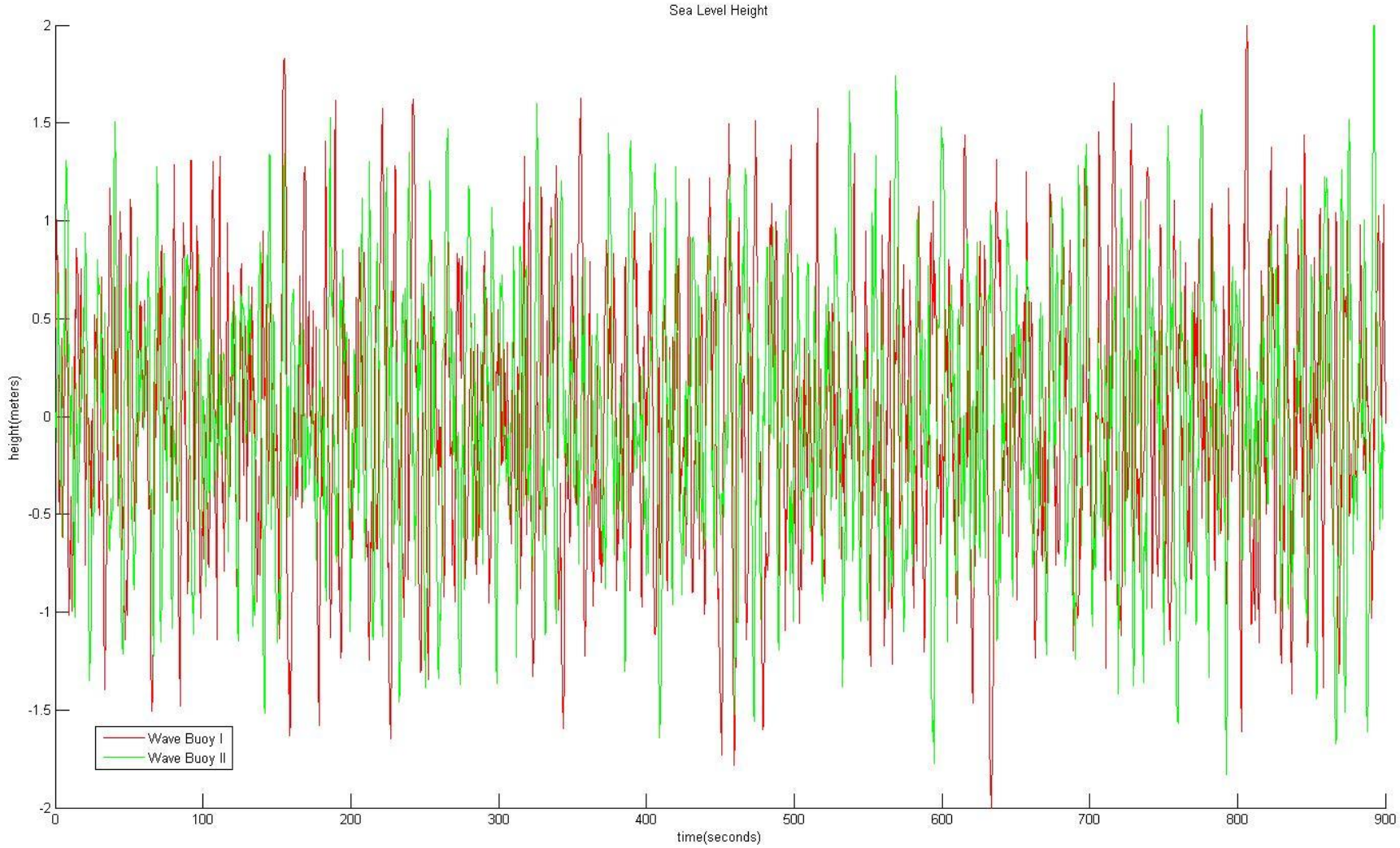

II. Resulting Graphs from each Calculation Example from Lag 4.